Xiao et al. BMC Musculoskeletal Disorders (2025) 26:466
https://doi.org/10.1186/s12891-025-08697-7

BMC Musculoskeletal Disorders

RESEARCH

Open Access

Rethinking femoral neck anteversion assessment: a novel automated 3D CT method compared to traditional manual techniques

Honghu Xiao[1], Sutuke Yibulayimu[2], Chunpeng Zhao[1*], Yudi Sang[3], Yimin Chen[1], Yufeng Ge[1], Qingnan Sun[1], Yang Ming[1], Mingjian Bei[1], Gang Zhu[3], Yingchun Song[3], Yu Wang[2] and Xinbao Wu[1]

Abstract

Purpose To evaluate the accuracy and reliability of a novel automated 3D CT-based method for measuring femoral neck anteversion (FNA) compared to three traditional manual methods.

Methods A total of 126 femurs from 63 full-length CT scans (35 men and 28 women; average age: 52.0 ± 14.7 years) were analyzed. The automated method used a deep learning network for femur segmentation, landmark identification, and anteversion calculation, with results generated based on two axes: Auto_GT (using the greater trochanter-to-intercondylar notch center axis) and Auto_P (using the piriformis fossa-to-intercondylar notch center axis). These results were validated through manual landmark annotation. The same dataset was assessed using three conventional manual methods: Murphy, Reikeras, and Lee methods. Intra- and inter-observer reliability were assessed using intraclass correlation coefficients (ICCs), and pairwise comparisons analyzed correlations and differences between methods.

Results The automated methods produced consistent FNA measurements (Auto_GT: 17.59 ± 9.16° vs. Auto_P: 17.37 ± 9.17° on the right; 15.08 ± 9.88° vs. 14.84 ± 9.90° on the left). Intra-observer ICCs ranged from 0.864 to 0.961, and inter-observer ICCs between Auto_GT and the manual methods were high, except for the Lee method. No significant differences were observed between the two automated methods or between the automated and manual verification methods. Moreover, strong correlations ($R > 0.9$, $p < 0.001$) were found between Auto_GT and the manual methods.

Conclusion The novel automated 3D CT-based method demonstrates strong reproducibility and reliability for measuring femoral neck anteversion, with performance comparable to traditional manual techniques. These results indicate its potential utility for preoperative planning, postoperative evaluation, and computer-assisted orthopedic procedures.

Clinical trial number Not applicable.

Keywords Femoral neck anteversion, 3D CT, Automated measurement, Deep learning

*Correspondence:
Chunpeng Zhao
zhaochunpeng_jst@163.com
[1]Department of Orthopaedics and Traumatology, Beijing Jishuitan Hospital, Capital Medical University, National Center for Orthopaedics, Beijing 100035, China
[2]Key Laboratory of Biomechanics and Mechanobiology, Ministry of Education, Beijing Advanced Innovation Center for Biomedical Engineering, School of Biological Science and Medical Engineering, Beihang University, Beijing, China
[3]Beijing Rossum Robot Technology Co., Ltd, Beijing, China

Introduction

Femoral neck anteversion (FNA), the angle between the femoral neck and shaft, reflects the natural torsion of the femur and plays a pivotal role in orthopedic care [1]. Accurate assessment of FNA is critical not only for diagnosing developmental and metabolic abnormalities of the lower extremities but also for planning surgical interventions. From reducing and fixing femoral fractures to addressing malalignment disorders, precise FNA measurements guide effective treatment strategies [2–4]. In femoral shaft fractures, rotational malunion ranks as the second most common complication, with Boscher et al. highlighting that functional hip outcomes are significantly impaired when femoral malrotation exceeds 14° compared to the contralateral side [5–8].

Over time, various imaging techniques—including fluoroscopy, ultrasound, computed tomography (CT), and magnetic resonance imaging (MRI)—have been employed to assess FNA [9]. Among these, CT-based methods are the most widely adopted in clinical practice due to their detailed visualization of bone structures. However, differences in anatomical landmark selection across methods lead to variability in measurement results [10–12]. Additionally, despite good overall consistency, intra- and inter-observer measurement errors remain a notable challenge [13].

The advent of robot-assisted orthopedic surgery has transformed the field by enabling unparalleled precision in intraoperative control and sophisticated preoperative planning [14–16]. Leveraging advanced computing and deep learning capabilities, robotic systems provide tools to address complex orthopedic challenges with greater accuracy and efficiency.

In response to these advancements, we developed a novel automated 3D CT-based method for measuring FNA, designed to deliver precise and consistent results using standard CT imaging data. To validate its performance, we compared this method with three established manual measurement techniques, analyzing correlations and differences among the approaches. Additionally, manual landmark annotations were performed to ensure the accuracy and reliability of the automated method.

Method

Data collection

CT scans of the lower extremities from 63 participants were obtained at Beijing Jishuitan Hospital, China. The sample included 35 males and 28 females, with an average age of 52.0 ± 14.7 years (range: 20–75 years), resulting in a total of 126 femur datasets. Participants with a history of trauma or orthopedic surgery were excluded. Ethics approval was obtained from the Institutional Review Board of our hospital (Approval No. 2022 – 143). All CT scans were performed using a 64-layer spiral CT scanner (Philips IQon-Spectral CT) under a standardized protocol. The scanning range extended from the T1 vertebra to the toes, with the following parameters: 120 kV, 150 mAs, 350 × 350 mm field of view, 512 × 512 matrix resolution, and 0.8 mm reconstructed slice thickness. The scans were acquired with participants in the supine position.

Fully automated femoral neck anteversion measurement method

Automated femur segmentation

A deep neural network with a five-level 3D U-Net architecture was trained to segment femurs from CT images using the nnU-Net framework, which incorporated standard preprocessing and augmentation techniques [17]. The training process employed a combination of Dice coefficient and cross-entropy as the loss function. The dataset consisted of 70 independent CT scans, each containing two femurs, including some with degenerative changes. Ground-truth segmentations were created using Materialise Mimics software, ensuring segmentation of only the outer bone surface.The model was trained for 1,000 epochs using the ADAM optimizer (learning rate: 0.001) and validated through five-fold cross-validation, achieving an average Dice Similarity Coefficient (DSC) of 0.989.

Post-processing steps involved connected component analysis to remove isolated regions, retaining only the femur. Surface models were generated using the marching cubes algorithm for downstream point cloud processing. The average runtime for segmentation and surface model generation was 7.9 s, depending on the hardware. All experiments were performed on a system equipped with an Intel i9-12900KS CPU, an NVIDIA RTX 3080Ti GPU, and 32 GB of memory, with the algorithms implemented in Python and the deep segmentation network built using the PyTorch framework.

Automated femoral landmark identification

Statistical Shape Models (SSMs) are deformable shape templates for point cloud data that can capture the major variations in shape information across datasets. Once established, these models can be adjusted to fit specific instances and propagate landmark annotations.

As illustrated in Fig. 1, we introduce an automated method for identifying femoral landmarks to accurately measure femoral data. The approach consists of three main steps: [1] constructing SSMs for the proximal and distal parts of the femur through non-rigid registration to establish point-to-point correspondences [2], annotating key anatomical landmarks and regions on the mean shape of the SSM, and [3] fitting the SSM to patient-specific geometries to propagate the landmarks and regions, which include the femoral head center (FHC)

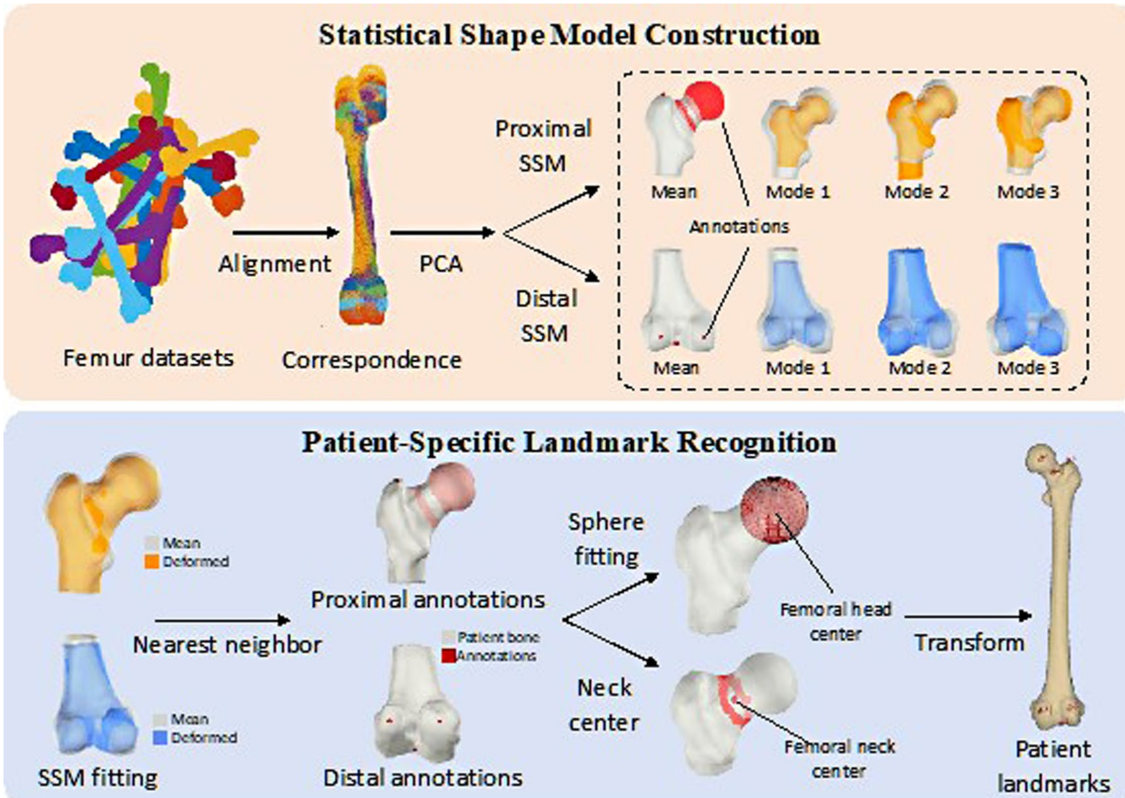

Fig. 1 Pipeline for automated femoral landmark identification using statistical shape models

and femoral neck center (FNC) derived from the corresponding regions.

Statistical shape model construction

SSMs for the proximal and distal parts of the femur were developed separately using a dataset of N femoral geometries $\{M_1, M_2, ., M_N, \}$, each represented as a surface point cloud. Initially, all surface points were normalized to a common coordinate system through rigid alignment, ensuring uniform orientation across the dataset. A non-rigid registration algorithm was then applied to deform each surface point M_i to align with a reference template [18]. The template was chosen arbitrarily, as the method was template-independent. The registration process optimizes a cost function that balances geometric alignment and local deformation smoothness, resulting in dense point-to-point correspondences across all surface points.

Once the correspondences were established, the aligned shapes $\{X_1, X_2, ..., X_N, \}$ were represented as vectors of surface point coordinates, with each vector X_i containing the 3D coordinates of all surface points. Principal component analysis (PCA) was applied to model the shape variability, resulting in the following representation:

$$X = \overline{X} + Pb$$

where $\overline{X}$ is the mean shape, P is a matrix of eigenvectors (the shape modes), and b is a vector of shape coefficients that describe individual shape variations. Adjusting the shape parameters b modifies the model's shape.

The SSMs were trained using the same dataset described in Sect. 1.1. Four anatomical landmarks, femoral head region, and femoral neck region, are marked on the mean template $\overline{X}$, so that they could be propagated to all shape variations.

Patient-specific landmark identification

An iterative optimization process was employed to map the SSM onto patient-specific femoral geometries y [19]. This process refined both the shape coefficients b and alignment transformation T to minimize the difference between the patient geometry and the deformed SSM. The optimization can be expressed as:

$$\widehat{b} = \text{argmin} \left\| T(y) - \bar{X} - Pb \right\|, \ \mid \text{b} \mid < \pm 3\lambda ,$$

where λ is the eigenvalues of the PCA components, constraining b to ensure that the generated shapes remain anatomically feasible.

After fitting the SSM to the patient-specific geometry, femoral landmarks were identified by mapping the SSM annotations to the corresponding points on the patient geometry. Since the FHC and FNC are located inside the bone, the related regions were first propagated, and the landmarks were calculated from those regions within the patient geometry. The FHC was then determined by fitting a sphere to the femoral head region, with the sphere's center defining the landmark. Similarly, the FNC was calculated by finding the centroid of the femoral neck region in the fitted SSM. The remaining landmarks, including the tip of greater trochanter (GT), the posterior aspects of the lateral femoral condyle (LFC) and the medial femoral condyle (MFC), and the intercondylar notch center (ICNC), were directly mapped from the annotated SSM template to the patient geometry. The average run time for identifying landmarks on a single case was 28.5 (20.7 to 39.3) s. Therefore, the total run time for processing a single femur CT was 36.4 (29.1 to 46.9) s.

Anteversion calculation using automated methods

After identifying the six femoral landmarks, the anteversion was calculated programmatically using Python. The femoral neck axis was defined by connecting the FHC and FNC, while the posterior condylar axis was established by linking the medial and lateral posterior condylar landmarks. To determine the anteversion, both axes were projected onto a plane perpendicular to the greater trochanter-to-intercondylar notch center (GT-ICNC) axis. The angle between the two projected lines was calculated, as illustrated in Fig. 2, and this approach was designated as the automated method based on the GT-ICNC axis (Auto_GT). The angle's sign was determined by evaluating the direction of the cross product of the two projected vectors relative to the GT-ICNC axis.

To assess the impact of alternative axis selection, the lateral edge of the piriformis fossa was mapped onto the annotated SSM template, and a piriformis anatomical axis was constructed by connecting this landmark to the ICNC. A second anteversion angle was then calculated using this piriformis anatomical axis, referred to as the automated method based on the piriformis anatomic axis (Auto_P). This approach allowed for evaluating the influence of different axis selections on the measurement outcomes.

Other measurement methods

To evaluate the reproducibility and reliability of the automated measurement methods, three clinically established manual measurement techniques were selected for comparison. The methods of Murphy et al. and Reikeras et al. are based on 2D axial CT slice [10, 11], while the method of Lee et al. utilizes 3D CT reconstructions [12]. In the conventional CT-based methods, FNA is measured from 2D information and projections along the CT-scan table axis. Both Murphy and Reikeras' methods utilize the posterior condylar axis, but the proximal femoral reference line differs between these methods. Murphy et al. define the proximal femoral neck axis as the line connecting the FHC and the center of the base of the femoral neck directly superior to the lesser trochanter [11]. In contrast, Reikeras et al. identify the femoral neck axis on an image where the anterior and posterior cortices are parallel [10].

The method of Lee et al. calculates the femoral neck center as the midpoint of the narrowest portion of the neck on each axial image, determined on both axial and coronal planes. The femoral head center is identified by fitting a circle to the femoral head's circumference on a series of orthogonal sectional views. The anteversion is then measured as the angle between the femoral neck axis and the posterior condylar axis on an axial plane parallel to the posterior condylar axis and perpendicular to the posterior femoral plane [12].

Additionally, the reproducibility of the automated methods was validated using a manual approach for the automated_GT method (Manual_GT). In this process,

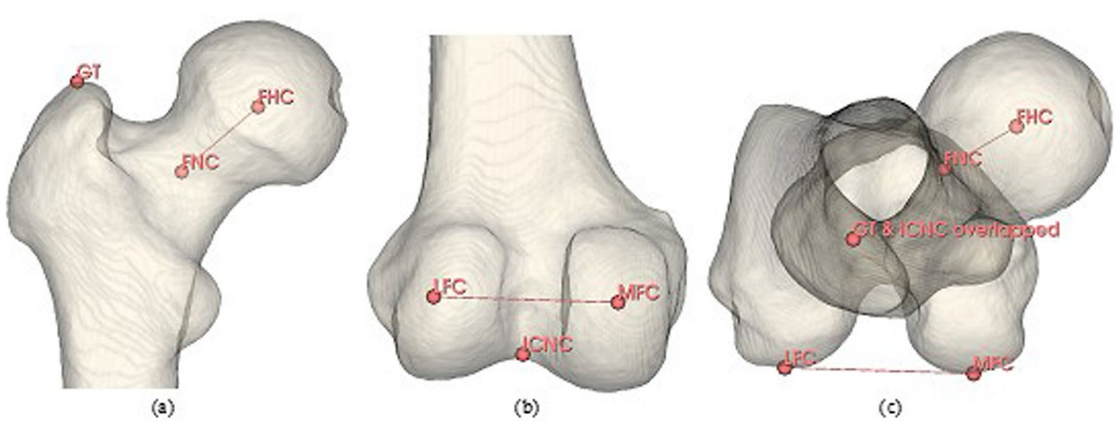

Fig. 2 Identified femoral landmarks and the definition of femoral anteversion. (**a**) Proximal part of femur. (**b**) Distal part of femur. (**c**) View along the GT-ICNC axis. FHC-femoral head center, FNC-femoral neck center, GT-greater trochanter, LFC-lateral femoral condyle, MFC-medial femoral condyle, ICNC-intercondylar notch center

the landmarks used in the automated method were annotated manually by two independent, blinded observers. The manual annotation process followed a pre-defined sequence: first by participant ID order and then by age order, over a period of two weeks. All annotations were performed using the 3D Slicer software, and calculations were implemented in Python.

Statistical analysis

Data analysis was conducted using SPSS 26.0 and R language (version 4.1.1). Normality was assessed using the Shapiro-Wilk test. Data with a normal distribution are presented as mean ± standard deviation, while non-normal data are expressed as medians and interquartile ranges.

Intra-observer reliability and inter-observer reproducibility were assessed using intraclass correlation coefficients (ICC), with results interpreted as follows: minimal (< 0.2), poor (0.21–0.4), moderate (0.41–0.6), strong (0.61–0.8), and almost perfect (> 0.8). Pairwise t-tests were used to compare different methods when normality criteria were met, while the Wilcoxon signed-rank test was applied for non-normally distributed data. Linear regression analysis was employed to evaluate differences among methods. Pearson correlation coefficients were graded as: very weak (< 0.2), weak (0.2–0.39), moderate (0.4–0.59), strong (0.6–0.79), and very strong (≥ 0.8). A two-sided p-value of < 0.05 was considered statistically significant.

Table 1 Four manual methods and two computer-based automated methods for bilateral FNA

Method	Assessment	FNA (°)	
		Mean ± SD	**Min-Max**
Right side			
Murphy	Manual	17.91 ± 9.19	1.62 to 37.7
Reikeras	Manual	14.39 ± 9.4	-1.61 to 35.96
Lee	Manual	11.04 ± 7.78	-1.26 to 30.13
Manual_GT	Manual	15.24 ± 8.77	-2.56 to 35.07
Auto_GT	Automated	17.59 ± 9.16	0.16 to 39.77
Auto_P	Automated	17.37 ± 9.17	0.15 to 39.29
Left side			
Murphy	Manual	15.13 ± 10.34	-8.49 to 37.18
Reikeras	Manual	11.09 ± 10.41	-12.31 to 33.81
Lee	Manual	8.25 ± 8.55	-9.04 to 28.43
Manual_GT	Manual	12.4 ± 9.55	-9.04 to 33.21
Auto_GT	Automated	15.08 ± 9.88	-6.86 to 37.02
Auto_P	Automated	14.84 ± 9.9	-7.03 to 36.79

Auto_GT automated method with GT-ICNC axis, *Auto_P* automated method with piriformis anatomic axis -ICNC axis, *Manual_GT* manual verification for automated_GT method

Result

All data were normally distributed, and the mean FNA measurements were summarized in Table 1. The results of the two automated methods were highly consistent, with values of 17.59 ± 9.16° for auto_GT and 17.37 ± 9.17° for auto_P on the right side, and 15.08 ± 9.88° for auto_GT and 14.84 ± 9.90° for auto_P on the left side (Table 1).

The intra-observer ICC demonstrated almost perfect agreement for both observers, with ranges of 0.864–0.961 and 0.853–0.964, respectively (Fig. 3a). Inter-observer ICCs for the manual methods were all above 0.75, as shown in Fig. 3b. When the means of two measurements taken by the observers were compared with the automated measurement results, the inter-observer ICCs between auto_GT and the manual methods were almost perfect, except for the comparison with the Lee method (Fig. 3c). A perfect agreement (ICC = 1) was observed between the two automated methods (auto_GT and auto_P) (Fig. 3d). The comparisons between the automated and manual methods revealed significant differences between specific combinations: Murphy vs. Lee, Lee vs. auto_GT, and Lee vs. auto_P, on both the left and right sides ($p < 0.001$, Fig. 4). However, no significant differences were found between the two automated methods, nor between the automated methods and the manual verification method (Fig. 4, Supplementary Table 1). Correlation analysis showed strong positive correlations ($R > 0.9$, $p < 0.001$) between the auto_GT method and the other methods (Fig. 5), further supporting the reliability and consistency of the automated approach.

Discussion

Accurate measurement of FNA is essential in orthopedic practice, particularly for diagnosing conditions such as hip dysplasia, impingement syndromes, and lower-extremity alignment abnormalities, as well as for planning procedures like hip arthroplasty and osteotomy. In the era of robot-assisted surgery, automating FNA measurement is increasingly important to enhance precision and support surgical management [15, 16]. Although various techniques have been developed [10–12, 20], discrepancies among methods highlight the need for more robust and standardized approaches.

Historically, 2D methods, including biplane X-rays, were favored for their low cost; however, they depend heavily on precise angles and positioning, which compromises reliability and consistency [9]. With the advent of CT imaging, FNA measurement became more accurate and reproducible due to improved contrast between bone and soft tissue [21]. Over time, 3D CT reconstruction techniques have further advanced FNA assessment by reducing the influence of subject positioning and allowing visualization in multiple planes [22]. For example, Lee et al. [12] introduced a 3D approach that refines

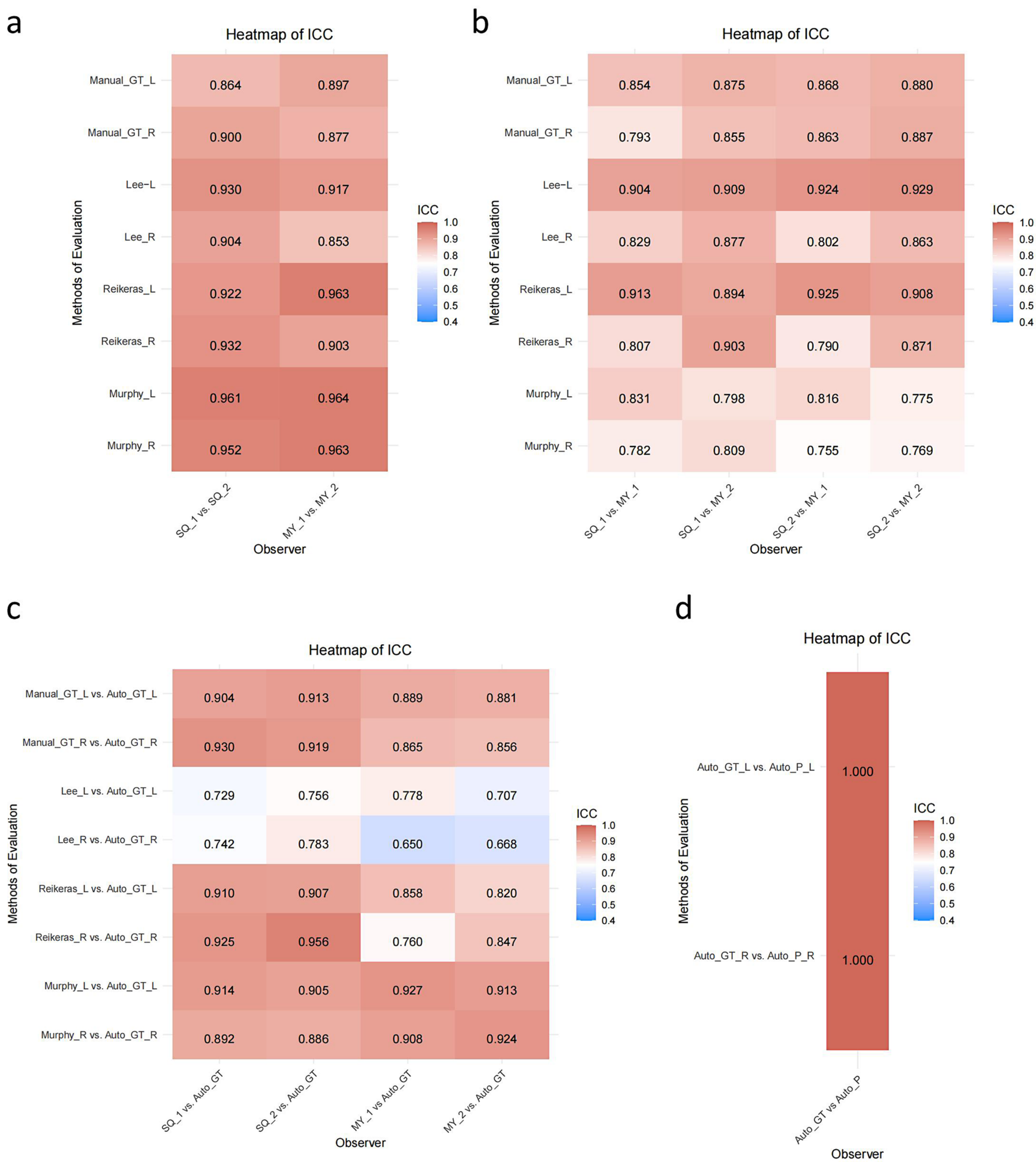

Fig. 3 Heatmap of intraclass correlation coefficients (ICC) for different methods. (**a**) Test-retest reliability of two observers using four manual measurement methods for bilateral FNA; (**b**) Inter-observer reproducibility between two observers using four manual measurement methods for bilateral FNA; (**c**) Inter-observer reproducibility between two observers using manual methods and a computer using Auto_GT for bilateral FNA; (**d**) Inter-observer reproducibility between two computer-based automatic methods for bilateral FNA;. *Auto_GT* automated method with GT-ICNC axis, *Auto_P* automated method with piriformis anatomic axis -ICNC axis, *Manual_GT* manual verification for automated_GT method, *ICC* intraclass correlation coefficients, *SQ_1* first measurement by the first observer, *SQ_2* second measurement by the first observer, *MY_1* first measurement by the second observer, *MY_2* second measurement by the second observer

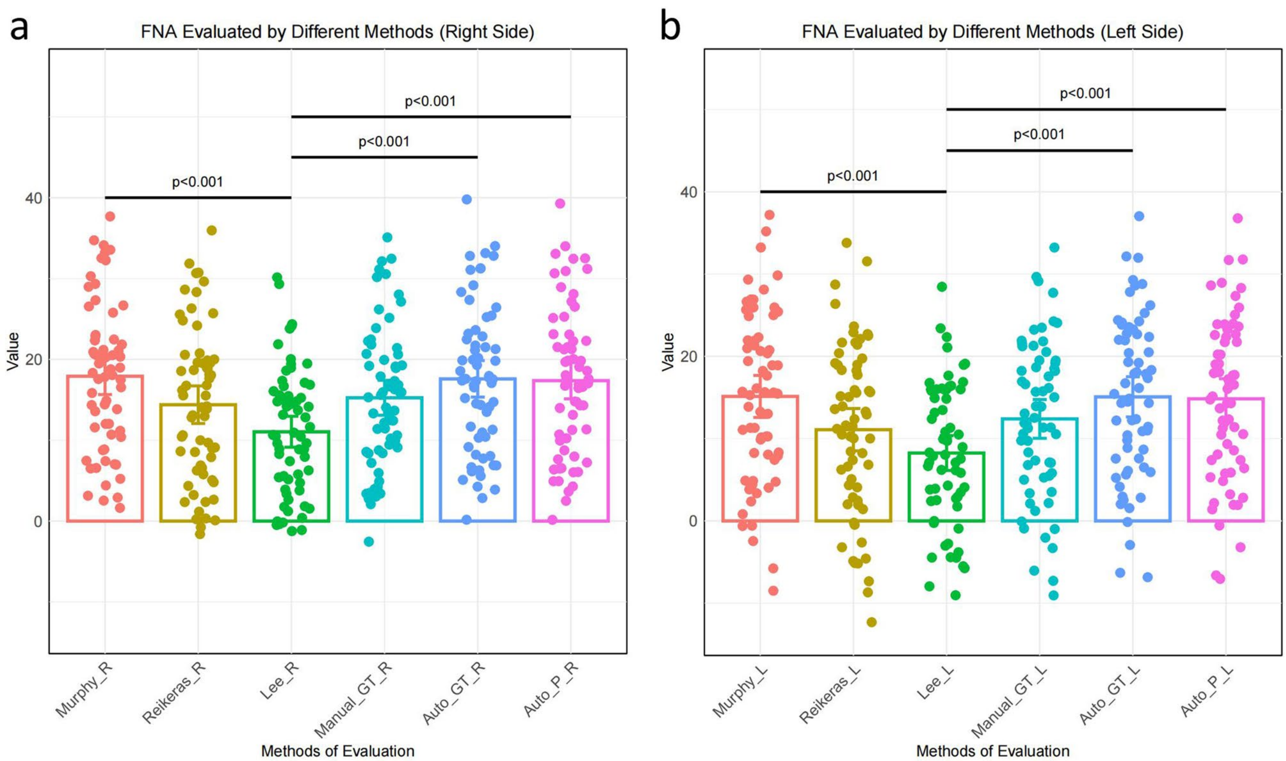

Fig. 4 Column-scatter plot of different methods. (**a**) Right side; (**b**) Left side;. *Auto_GT* automated method with GT-ICNC axis, *Auto_P* automated method with piriformis anatomic axis -ICNC axis, *Manual_GT* manual verification for automated_GT method

landmark annotation via a simulated posterior femoral plane, while Sangeux et al. [23] proposed an oblique axial view for defining the femoral neck axis. Despite these advances, both 2D and 3D methods still rely on manual selection of anatomical landmarks, which can introduce inter- and intra-observer variability.

In comparison, our novel fully automated method offers several advantages in this evolving technological landscape. By leveraging SSM technique, our approach automatically identifies key anatomical landmarks and measures FNA without manual intervention [24]. This automation minimizes potential measurement errors associated with subjective landmark selection and enhances reproducibility. Furthermore, the fully automated process facilitates seamless integration with robotic-assisted surgical planning systems, making it a promising tool for modern orthopedic practice.

In this study, we compared the automated measurement method with three established manual methods to assess its feasibility and accuracy. To further validate the automated approach, we conducted manual landmark annotations and evaluated the reliability and reproducibility of the automated methods using two axes: the GT-ICNC axis and the piriformis fossa-to-ICNC axis. The mean manual measurements ranged from approximately 12° to 15°, aligning closely with values reported in historical literature [10–12]. However, among the manual methods, the Murphy method yielded the highest FNA values, while the Lee method produced the lowest. These findings align with previous studies, such as those by Schmaranzer et al. [13], which highlight similar discrepancies across methods. Consistent with Dimitriou et al. [25], we observed asymmetry in FNA measurements between the left and right femurs within the normal range. High intra-observer and inter-observer reliability were achieved, though significant differences were noted between manual methods and between manual and automated measurements. The perfect correlation between the two axes further confirm the validity of using the GT-ICNC axis as a reliable reference.

The differences in FNA measurements across studies can often be attributed to variations in landmark selection. Kim et al. [22] identified three primary sources of error: the posterior-most condylar axis, the femoral neck axis, and the femoral shaft axis. The femoral head, although nearly spherical, features a medial depression (fovea capitis femoris) that complicates precise landmark identification [26]. Femoral neck's radially asymmetric cross-section makes it challenging to accurately define the center using biplane projections. The Murphy and Reikeras methods, which mark the femoral neck base and center on a single axial plane, have greater inter-observer and intra-observer variability due to ambiguous landmark definitions [10, 11].

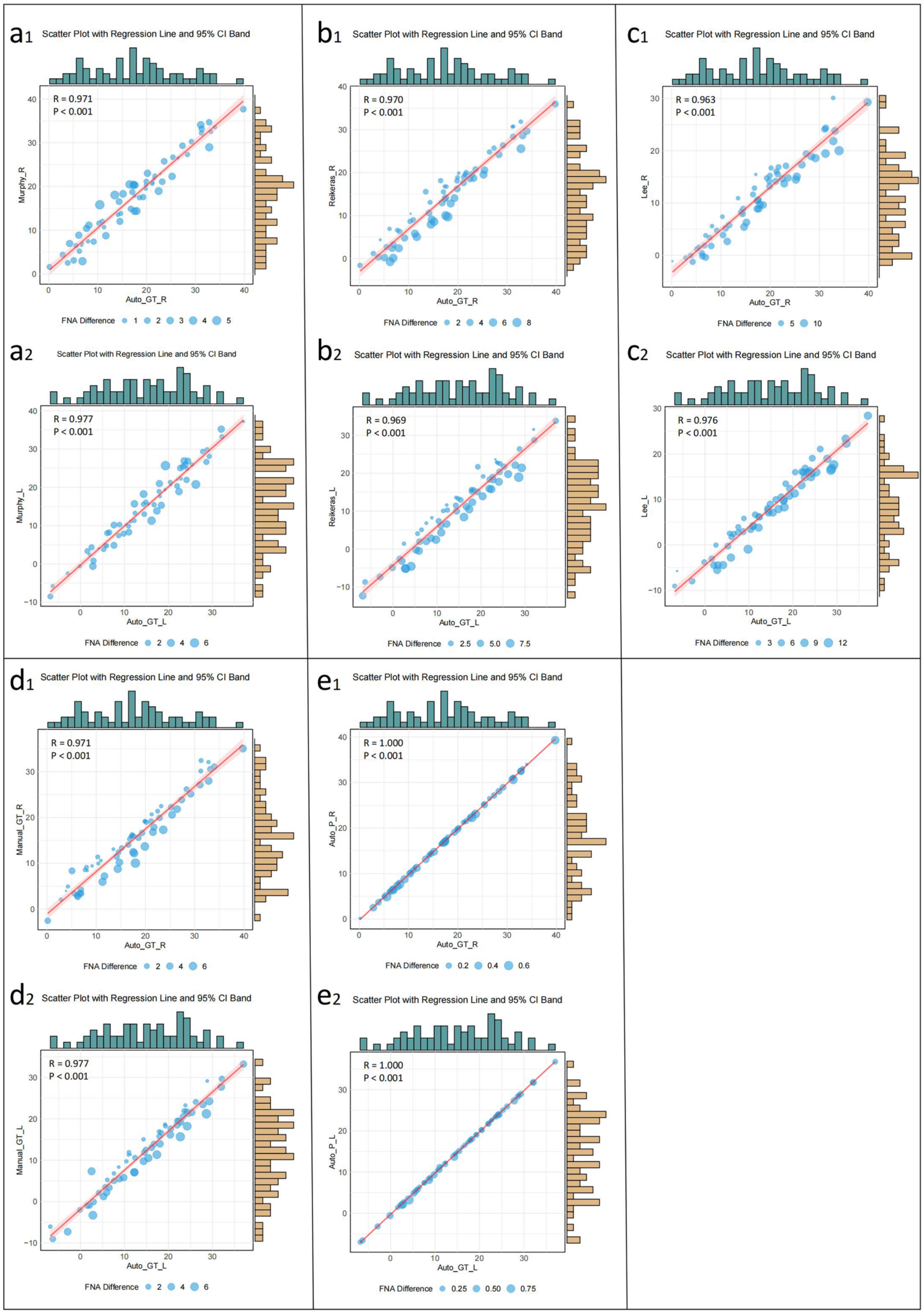

Fig. 5 Scatter plot and linear regression analysis of manual and automatic assessments. (**a**) Auto_GT vs. Murphy Method; (**b**) Auto_GT vs. Reikeras Method; (**c**) Auto_GT vs. Lee Method; (**d**) Auto_GT vs. Manual_GT; (**e**) *Auto_GT* vs. Auto_P. *Auto_GT* automated method with GT-ICNC axis, Auto_P automated method with piriformis anatomic axis -ICNC axis, Manual_GT manual verification for automated_GT method

The posterior condyles of the distal femur also present challenges in landmark identification. While largely spherical, the medial condyle has an inferior facet with a larger sagittal radius [27]. Traditional approaches, which define the posterior condylar axis using the apexes of the medial and lateral condyles, are prone to variability when measured on separate axial planes. Recent studies by Davis et al. and Castagnini et al. suggest using the transepicondylar axis as the distal landmark for FNA measurement due to its higher reliability [28, 29]. Consistent with most studies, our method adopted the posterior condylar axis as the distal landmark. While identifying landmarks using angles in a 2D plane is simpler, our results demonstrate that 3D landmark identification is feasible and more closely mimics cadaveric specimen manipulation [22].

In conventional methods, CT scans are assumed to align with the femoral shaft axis, a condition rarely achieved in clinical practice. The anatomical axis of the distal femur differs from the proximal axis in both coronal and sagittal planes [30]. This discrepancy underscores the lack of consensus on defining a single axis connecting the proximal and distal femur. Some researchers define the axis based on the intercondylar fossa or the femoral shaft center on axial slices near the lesser trochanter [23, 31], while others, such as Lee et al., use the mechanical axis [12]. Our findings indicate that a 1° deviation in the femoral axis results in an FNA measurement error of 0.5° to 2° within the common range (10°–20°). These results align with Wu's findings [32], which demonstrated a strong correlation ($r > 0.9$) between the piriformis anatomical axis and clinical anatomical axis for lower extremity alignment.

Notably, the lateral edge of the piriformis fossa, a key entry point for antegrade intramedullary nailing of the femur, serves as an alternative landmark. While manual methods often rely on the tip of the greater trochanter—a landmark easily preserved after intramedullary nailing or hip arthroplasty—our results confirm that automated measurements using either landmark result in an error of less than 0.25°.

This study has several limitations. First, our CT data were sourced from a clinical practice database, and the accuracy of the method in extreme FNA values or pathological cases has not been evaluated; its performance in femurs with severe deformities or prior surgeries remains to be determined. Second, while the SSM facilitates automated landmark detection, it is based on population-specific anatomical data, which may limit its generalizability to diverse demographics. Lastly, the study exclusively included adult subjects, thereby excluding pediatric cases and elderly individuals with significant degenerative changes, potentially affecting the broader applicability of our findings. Further validation in more diverse populations is warranted.

Conclusion

This study introduces a novel, automated 3D CT-based method for FNA measurement, demonstrating high reproducibility and reliability. By minimizing errors from manual measurements and non-parallel scanning, this method provides accurate and consistent results. Its ease of implementation on common computing platforms makes it a promising tool for preoperative planning, postoperative evaluation, and future applications in robotic-assisted orthopedic surgeries, offering significant potential to enhance clinical precision and outcomes.

Abbreviations

FNA	Femoral neck anteversion
CT	Computed tomography
MRI	Magnetic resonance imaging
DSC	Dice Similarity Coefficient
SSMs	Statistical Shape Models
FHC	Femoral head center
FNC	Femoral neck center
GT	Greater trochanter
LFC	Lateral femoral condyle
MFC	Medial femoral condyle
ICNC	Intercondylar notch center
GT-ICNC	Greater trochanter-to-intercondylar notch center
ICC	Intraclass correlation coefficients
Auto_GT	Automated method with GT-ICNC axis
Auto_P	Automated method with piriformis anatomic axis -ICNC axis
Manual_GT	Manual verification for automated_GT method

Supplementary Information

The online version contains supplementary material available at https://doi.org/10.1186/s12891-025-08697-7.

Supplementary Material 1

Author contributions

Conceptualization: H.X., C.Z.; Data curation: H.X., Y.S.; Formal analysis, investigation, and methodology: Y.C., M.B.; Funding acquisition: H.X., C.Z.; Supervision: X.W., Y.W.; Writing—original draft: H.X., Y.G., S.Y., Y.S., and Y.C.; Writing—review & editing: Y.G., Y.S. All authors have read and agreed to the published version of the manuscript.

Funding

This work was supported in part by the Beijing Hospitals Authority Clinical Medicine Development of special funding support, code: YGLX202512, Beijing Jishuitan Research Funding (ZR-202504), National Natural Science Foundation of China (Grant no. 62471322), and Natural Science Foundation of Beijing (L222136).

Data availability

The datasets used in this study are not publicly available because of patient confidentiality but are available from the corresponding author on reasonable request.

Declarations

Ethics approval

Approval was obtained from the institutional review boards of the Beijing Jishuitan Hospital (Approval No. 2022 – 143), and all procedures used adhere to the tenets of the Declaration of Helsinki.

Consent for publication

Not applicable.

Consent to participate

Informed consent was obtained from all individual participants included in the study.

Competing interests

The authors declare no competing interests.

Received: 11 December 2024 / Accepted: 24 April 2025
Published online: 13 May 2025

References

1. Cibulka MT. Determination and significance of femoral neck anteversion. Phys Ther. 2004;84(6):550–8.
2. Leonardi F, Rivera F, Zorzan A, Ali SM. Bilateral double osteotomy in severe torsional malalignment syndrome: 16 years follow-up. J Orthop Traumatol. 2014;15(2):131–6.
3. Souza AD, Ankolekar VH, Padmashali S, Das A, Souza A, Hosapatna M. Femoral neck anteversion and neck shaft angles: determination and their clinical implications in fetuses of different gestational ages. Malays Orthop J. 2015;9(2):33–6.
4. Su Y, Chen K, Wu J, Zhu J, Chen X. Femoral version and its clinical relevance in adult hip preservation surgery for developmental dysplasia of the hip. EFORT Open Rev. 2024;9(9):873–82.
5. Langer JS, Gardner MJ, Ricci WM. The cortical step sign as a tool for assessing and correcting rotational deformity in femoral shaft fractures. J Orthop Trauma. 2010;24(2):82–8.
6. Citak M, Suero EM, O'Loughlin PF, Arvani M, Hufner T, Krettek C, et al. Femoral malrotation following intramedullary nailing in bilateral femoral shaft fractures. Arch Orthop Trauma Surg. 2011;131(6):823–7.
7. Branca Vergano L, Coviello G, Monesi M. Rotational malalignment in femoral nailing: prevention, diagnosis and surgical correction. Acta Biomed. 2020;91(14–s):e2020003.
8. Boscher J, Alain A, Vergnenegre V, Hummel G, Charissoux JL, Marcheix PS. Femoral shaft fractures treated by antegrade locked intramedullary nailing: EOS stereoradiographic imaging evaluation of rotational malalignment having a functional impact. Orthop Traumatol Surg Research: OTSR. 2022;108(5):103235.
9. Scorcelletti M, Reeves ND, Rittweger J, Ireland A. Femoral anteversion: significance and measurement. J Anat. 2020;237(5):811–26.
10. Reikeras O, Bjerkreim I, Kolbenstvedt A. Anteversion of the acetabulum and femoral neck in normals and in patients with osteoarthritis of the hip. Acta Orthop Scand. 1983;54(1):18–23.
11. Murphy SB, Simon SR, Kijewski PK, Wilkinson RH, Griscom NT. Femoral anteversion. J Bone Joint Surg Am Volume. 1987;69(8):1169–76.
12. Lee YS, Oh SH, Seon JK, Song EK, Yoon TR. 3D femoral neck anteversion measurements based on the posterior femoral plane in ORTHODOC system. Med Biol Eng Comput. 2006;44(10):895–906.
13. Schmaranzer F, Lerch TD, Siebenrock KA, Tannast M, Steppacher SD. Differences in femoral torsion among various measurement methods increase in hips with excessive femoral torsion. Clin Orthop Relat Res. 2019;477(5):1073–83.
14. Zhu Q, Liang B, Wang X, Sun X, Wang L. Minimally invasive treatment of displaced femoral shaft fractures with a teleoperated robot-assisted surgical system. Injury. 2017;48(10):2253–9.
15. Zhao C, Cao Q, Sun X, Wu X, Zhu G, Wang Y. Intelligent robot-assisted minimally invasive reduction system for reduction of unstable pelvic fractures. Injury. 2023;54(2):604–14.
16. Zhao C, Xiao H, Cao Q, Ge Y, Li Y, Wang Y, et al. Innovative development of robot reduction system in geriatric pelvic fractures: A single-center case series in Beijing, China. J Orthop Translation. 2024;49:283–8.
17. Isensee F, Jaeger PF, Kohl SAA, Petersen J, Maier-Hein KH. nnU-Net: a self-configuring method for deep learning-based biomedical image segmentation. Nat Methods. 2021;18(2):203–11.
18. Audenaert EA, Van Houcke J, Almeida DF, Paelinck L, Peiffer M, Steenackers G, et al. Cascaded statistical shape model based segmentation of the full lower limb in CT. Comput Methods Biomech Biomed Engin. 2019;22(6):644–57.
19. Yibulayimu S, Liu Y, Sang Y, Zhu G, Wang Y, Liu J, et al. editors. Pelvic fracture reduction planning based on morphable models and structural constraints. Medical image computing and computer assisted Intervention – MICCAI 2023; 2023 2023//; Cham: Springer Nature Switzerland.
20. Cheng XG, Nicholson PH, Boonen S, Brys P, Lowet G, Nijs J, et al. Effects of anteversion on femoral bone mineral density and geometry measured by dual energy X-ray absorptiometry: a cadaver study. Bone. 1997;21(1):113–7.
21. Beebe MJ, Wylie JD, Bodine BG, Kapron AL, Maak TG, Mei-Dan O, et al. Accuracy and reliability of computed tomography and magnetic resonance imaging compared with true anatomic femoral version. J Pediatr Orthop. 2017;37(4):e265–70.
22. Kim JS, Park TS, Park SB, Kim JS, Kim IY, Kim SI. Measurement of femoral neck anteversion in 3D. Part 1: 3D imaging method. Med Biol Eng Comput. 2000;38(6):603–9.
23. Sangeux M, Pascoe J, Graham HK, Ramanauskas F, Cain T. Three-dimensional measurement of femoral neck anteversion and neck shaft angle. J Comput Assist Tomogr. 2015;39(1):83–5.
24. Johnson LG, Bortolussi-Courval S, Chehil A, Schaeffer EK, Pawliuk C, Wilson DR, et al. Application of statistical shape modeling to the human hip joint: a scoping review. JBI Evid Synth. 2023;21(3):533–83.
25. Dimitriou D, Tsai TY, Yue B, Rubash HE, Kwon YM, Li G. Side-to-side variation in normal femoral morphology: 3D CT analysis of 122 femurs. Orthopaedics & traumatology, surgery & research: OTSR. 2016;102(1):91–7.
26. Steppacher SD, Tannast M, Werlen S, Siebenrock KA. Femoral morphology differs between deficient and excessive acetabular coverage. Clin Orthop Relat Res. 2008;466(4):782–90.
27. Monk AP, Choji K, O'Connor JJ, Goodfellow JW, Murray DW. The shape of the distal femur: a geometrical study using MRI. Bone Joint J. 2014;96–B(12):1623–30.
28. Castagnini F, Giardina F, Tassinari E, Biondi F, Bracci G, Traina F. Measuring stem anteversion after total hip arthroplasty: posterior condylar tangent versus transepicondylar axis. Skeletal Radiol. 2021;50(9):1775–9.
29. Davis E, LeBrun DG, McCarthy T, Westrich GH. Femoral neck anteversion: which distal femur landmark matters? Arthroplast Today. 2024;26:101318.
30. Yazdi H, Nazarian A, Kwon JY, Hochman MG, Pakdaman R, Hafezi P, et al. Anatomical axes of the proximal and distal halves of the femur in a normally aligned healthy population: implications for surgery. J Orthop Surg Res. 2018;13(1):21.
31. Berryman F, Pynsent P, McBryde C. A semi-automated method for measuring femoral shape to derive version and its comparison with existing methods. Int J Numer Method Biomed Eng. 2014;30(11):1314–25.
32. Wu CC. Is clinical measurement of anatomic axis of the femur adequate? Acta Orthop. 2017;88(4):407–10.

Publisher's note